UCLA
UCLA Previously Published Works

Title
Copper Ion Binding Site in β-Amyloid Peptide

Permalink

Journal
Nano Letters, 16(10)

ISSN
1530-6984

Authors
Yugay, Diana
Goronzy, Dominic P
Kawakami, Lisa M
et al.

Publication Date
2016-10-12

DOI
10.1021/acs.nanolett.6b02590

Peer reviewed

Copper Ion Binding Site in β-Amyloid Peptide

Diana Yugay,[†,‡] Dominic P. Goronzy,[†,‡] Lisa M. Kawakami,[‡] Shelley A. Claridge,[‡,§,‖] Tze-Bin Song,[⊥] Zhongbo Yan,[⊥] Ya-Hong Xie,*[,†,⊥] Jérôme Gilles,*[,▽] Yang Yang,*[,†,⊥] and Paul S. Weiss*[,†,‡,⊥]

[†]California NanoSystems Institute, University of California, Los Angeles, Los Angeles, California 90095, United States

[‡]Department of Chemistry and Biochemistry, University of California, Los Angeles, Los Angeles, California 90095, United States

[§]Department of Chemistry and [‖]Weldon School of Biomedical Engineering, Purdue University, West Lafayette, Indiana 47907, United States

[⊥]Department of Materials Science and Engineering, University of California, Los Angeles, Los Angeles, California 90095, United States

[▽]Department of Mathematics and Statistics, San Diego State University, San Diego, California 92182, United States

Ⓢ *Supporting Information*

ABSTRACT: β-Amyloid aggregates in the brain play critical roles in Alzheimer's disease, a chronic neurodegenerative condition. Amyloid-associated metal ions, particularly zinc and copper ions, have been implicated in disease pathogenesis. Despite the importance of such ions, the binding sites on the β-amyloid peptide remain poorly understood. In this study, we use scanning tunneling microscopy, circular dichroism, and surface-enhanced Raman spectroscopy to probe the interactions between Cu^{2+} ions and a key β-amyloid peptide fragment, consisting of the first 16 amino acids, and define the copper−peptide binding site. We observe that in the presence of Cu^{2+}, this peptide fragment forms β-sheets, not seen without the metal ion. By imaging with scanning tunneling microscopy, we are able to identify the binding site, which involves two histidine residues, His13 and His14. We conclude that the binding of copper to these residues creates an interstrand histidine brace, which enables the formation of β-sheets.

KEYWORDS: scanning tunneling microscopy, Alzheimer's disease, β-amyloid, β-sheet, binding site, histidine brace
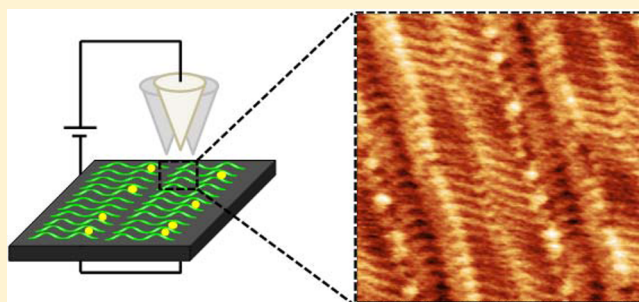
Alzheimer's disease (AD) is a worldwide health problem and the third most financially costly disease in the U.S. and Europe.[1] The dominant symptom of AD is anterograde amnesia and 60−80% of dementing illness is caused by AD.[2] A hallmark of AD is the aggregation of β-amyloid peptides (Aβ). Nevertheless, the body of knowledge around the disease pathogenesis is limited, the etiology remains poorly understood, and no curative interventions are available. It has been shown that people with AD exhibit abnormally high concentrations of transition metal ions (Cu^{2+} and Zn^{2+}) in Aβ aggregates and synaptic areas of the brain.[3−6] Nonetheless, the significance of Aβ interaction with metal ions for the disease process remains largely unexplored, and there remains no cure for AD. Better understanding of the structure(s) of Aβ peptides, their interactions with transition metals, and more precise definitions of the metal-peptide binding sites promise improved insight into AD and provide new avenues for treatment.

Aβ oligomers are considered to be neurotoxic through a variety of mechanisms, that is, interactions with cell membranes and the production of reactive oxygen species.[7−9] The pathway of Aβ neurotoxicity remains unknown and is the subject of active research. In prior work, Aβ has been shown to bind Cu^{2+} ions in 1:1 stoichiometric ratios in the vicinity of the N-terminus.[10] A second low-affinity binding site has also been suggested due to the binding of Cu^{2+} to Aβ in 1:2 stoichiometric ratios in the vicinity of the C-terminus.[10,11] The structure and the binding site of Aβ oligomers in the presence of metal ions have been extensively studied using nuclear magnetic resonance,[14] X-ray absorption spectroscopy,[12,15] Fourier transform infrared spectroscopy,[13] electron paramagnetic resonance,[16] and atomic force microscopy.[17,18] However, there is a paucity of experimental data with submolecular resolution because identifying exact amino acid involvement in metal ion binding is challenging due to the high mechanical and conformational flexibility of Aβ as well as the dramatic changes in conformation of the peptide based on metal ion valence.[5,19,20]

Previously, we have demonstrated the ability to resolve submolecular structures of biological molecules and to differentiate between side chains of individual amino acids and their orientations using scanning tunneling microscopy (STM) and related spectroscopic imaging methods.[21] In this

study, we report structural elucidation of the first 16 amino acids (1−16) of the full length Aβ and its structural variation in the presence (Aβ$_{1−16}$-Cu^{2+}) and the absence (Aβ$_{1−16}$) of Cu^{2+} ions via STM, surface-enhanced Raman spectroscopy (SERS), and circular dichroism (CD). We chose Cu^{2+} for this study due to its biological significance in AD.[13,22] Although Aβ$_{1−16}$ has been reported as a disordered region of Aβ and therefore is often *omitted* from computational studies,[23−27] our findings indicate that upon codeposition of Cu^{2+} and Aβ$_{1−16}$ on highly oriented pyrolytic graphite (HOPG), it laminates into structured β-sheet domains. We targeted this segment because preliminary data on Aβ$_{1−42}$ indicated binding of Cu^{2+} in this region.[10,13,18] Previous reports on the binding site of Cu^{2+} in this portion of the peptide are conflicting. Li and co-workers, based primarily on nuclear magnetic resonance (NMR) measurements, report the involvement of residues His6, His13, His 14, and Tyr10 in binding in Aβ$_{1−16}$, whereas Viles and co-workers, using a combination of NMR measurements and electron paramagnetic resonance (EPR) measurements, found that His13 is crucial for binding in Aβ$_{1−28}$ and there are indications of the involvement of His6 and His14, but *not* Tyr10.[28,29] Furthermore, these reports rely on conventional ensemble (i.e., averaging) measurements (NMR and EPR), whereas STM can provide definitive real-space images of noncrystalline, nonperiodic, and even dilute structures.[30] These results could significantly enhance our understanding of the biology of Aβ peptides in vivo and their morphological changes due to interactions with the synaptic cell membrane.[31−33] Most importantly, on the basis of the STM image analysis of the length and position of the protruding features, we determine and elucidate the specific interactions and binding of Cu^{2+} with Aβ$_{1−16}$. Here, we show that Cu^{2+} ions participate in interstrand Aβ$_{1−16}$ binding by coordinating with the two histidine residues at positions 13 and 14 (His13 and His14) on adjacent strands, and not intrastrand binding as had been hypothesized previously.[16,19,20]

Circular Dichroism. We used circular dichroism (CD) to determine whether Cu^{2+} ion binding onto Aβ$_{1−16}$ occurs readily in solution. In Figure S1, two bands (negative band at 197 nm and positive band at 222 nm) indicate that the polyproline type II (PPII) helix secondary structure conformation appears in the CD spectra of Aβ$_{1−16}$ at pH 7.4. The PPII helix structure is commonly found in many proteins in unfolded states.[34,35] The addition of Cu^{2+} to the solution decreased the CD spectra intensity in both bands. This indicates that Cu^{2+} weakens the PPII helical conformation and induces a partial β-sheet conformation in the peptide.[36,37] Because of its hydrophilicity, Aβ$_{1−16}$ is able to form hydrogen bonds with surrounding water molecules, which stabilizes the structure of the PPII helix.[34,38] A decrease in the number of water molecules around the PPII helix backbone causes the peptide to change its conformation from a PPII helix to a β-sheet.[39] Hence, the presence of Cu^{2+} around Aβ$_{1−16}$ may not only alter the Aβ$_{1−16}$ structure by binding but also cause the peptide to undergo a conformational change from a helix to a β-sheet by displacing water molecules around the peptide backbone.[40−43] The latter process is reported to be highly entropically favorable.[39,40] Though CD data alone do not enable making definitive structural assignments, they do indicate that structural changes occur upon binding Cu^{2+}.

Surface-Enhanced Raman Spectroscopy. The challenge of many infrared spectroscopy (IR) techniques when used to study biomolecular conformation on surfaces is their limited ability to investigate the structures of biomolecules at low concentrations.[44] An additional challenge for peptides and proteins is that the amide bands, which are responsible for the secondary structure, are located in the same region as the strong absorption band of water.[45] The infrared spectroscopy dependence on concentration imposes a significant barrier to studying amyloid peptides because they exhibit structural polymorphism, which is greatly influenced by concentration.[42,46] To overcome the above-mentioned challenges of IR techniques, and to stay consistent with Aβ$_{1−16}$ concentrations used throughout the scanning probe microscopy experiments, surface-enhanced Raman spectroscopy (SERS)[47] was employed to study conformational changes of Aβ$_{1−16}$ in the presence and absence of Cu^{2+}. Furthermore, to increase the intensity of the SERS signal, specialized platforms that exhibit large electromagnetic enhancements ($\sim10^{14}$) have been used, as shown in Figure 1a.[48−50]
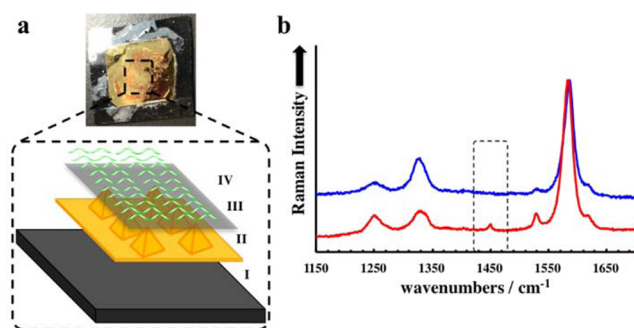

Figure 1. Substrate arrangement and results of the surface-enhanced Raman spectroscopy experiments. (a) (Top) Photograph of the substrate used in SERS experiments. (Bottom) Schematic of the substrate and its components: (I) silicon wafer, (II) gold film with gold pyramids, (III) graphene, (IV) deposited Aβ$_{1−16}$ peptides. (b) SERS spectrum of Aβ$_{1−16}$-Cu^{2+} (blue) and Aβ$_{1−16}$ (red). The black dashed box (~1449 cm$^{−1}$) indicates the C−H bending mode that signifies Aβ$_{1−16}$ peptides lack structural homogeneity in comparison to Aβ$_{1−16}$-Cu^{2+}.

Surface-enhanced Raman spectra for Aβ$_{1−16}$ and Aβ$_{1−16}$-Cu^{2+} are shown in Table 1 and Figure 1b. Changes in the secondary

Table 1. Vibrational Peak Positions and Corresponding Band Assignments for the Surface-Enhanced Raman Spectroscopy Spectra Recorded

Raman shift (cm$^{−1}$)	assignment	reference
1585	Graphene G band	53, 54
1529	Amide II band	55−60
1449	C−H bending mode	65−68
1328	Graphene D band	53, 54
1250	Amide III band	61−64

structure of Aβ$_{1−16}$ upon addition of Cu^{2+} ions were assessed based on displacement and intensity of the amide bands and the C−H bending vibrations of the peptide.

The Amide I band (1610−1700 cm$^{−1}$)[51,52] was not resolved by SERS due to overlap with the strong G band ~1585 cm$^{−1}$,[53,54] which comes from the graphene coating of the substrate surface (Figure 1). Because of its weak Raman activity there is little information available about the Amide II band,[55−58] yet a few reports mention that its location at ~1529 cm$^{−1}$ is associated with a β-sheet structure.[59,60] The
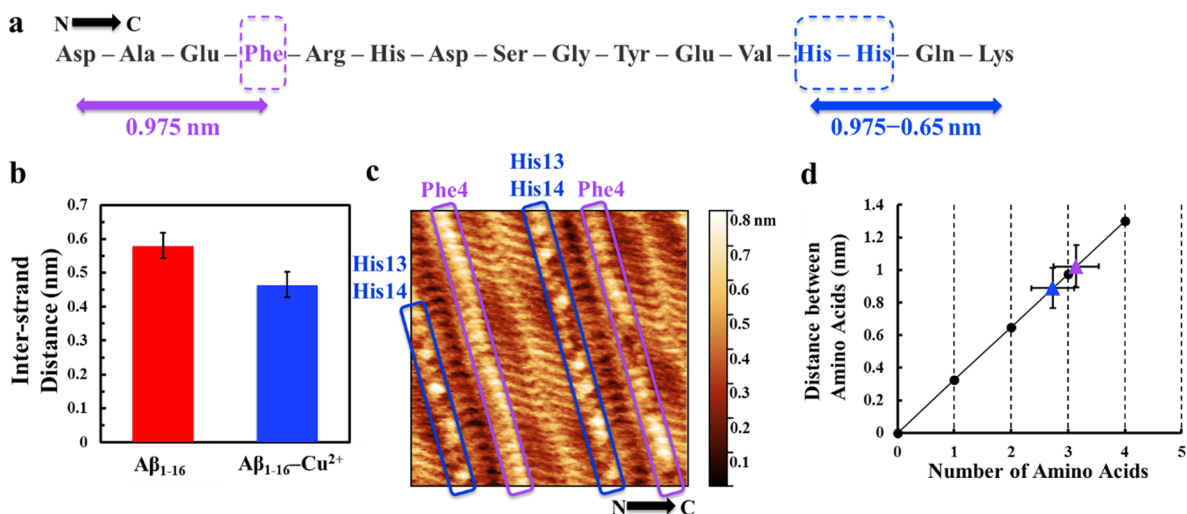
Figure 2. (a) $A\beta_{1-16}$ sequence with the highlighted Phe4 and His13/His14 amino acids. Ideal distance from β-sheet boundary to Phe4 is 0.975 nm (purple arrow), to His13 is 0.975 nm (blue arrow), and to His14 is 0.65 nm (blue arrow). (b) Average interstrand separation bar graph for $A\beta_{1-16}$ vs $A\beta_{1-16}$-Cu^{2+}. Interstrand separation for $A\beta_{1-16}$ is 5.8 ± 0.4 Å, and $A\beta_{1-16}$-Cu^{2+} is 4.6 ± 0.3 Å (from n = 42 and 120 measurements, respectively). (c) Scanning tunneling microscopy image of $A\beta_{1-16}$-Cu^{2+}. The regular protruding features in the purple box indicate the positions of the Phe4, whereas irregular protruding features in the blue box indicate the positions of His13/His14 binding Cu^{2+} in the peptide β-sheet assembly. Imaging conditions: V_{sample} = 0.55 V, I_{tunnel} = 10 pA. (d) Average distance between amino acids with the corresponding number of amino acids to the specified distance. Phe4 (purple) distance, 1.0 ± 0.1 nm; number of amino acids, 3.1 ± 0.4; His13/His14 (blue) distance, 0.9 ± 0.1 nm; number of amino acids, 2.7 ± 0.4; and ideal distance vs number of amino acids (black) (from n = 92 and 145 measurements, respectively).

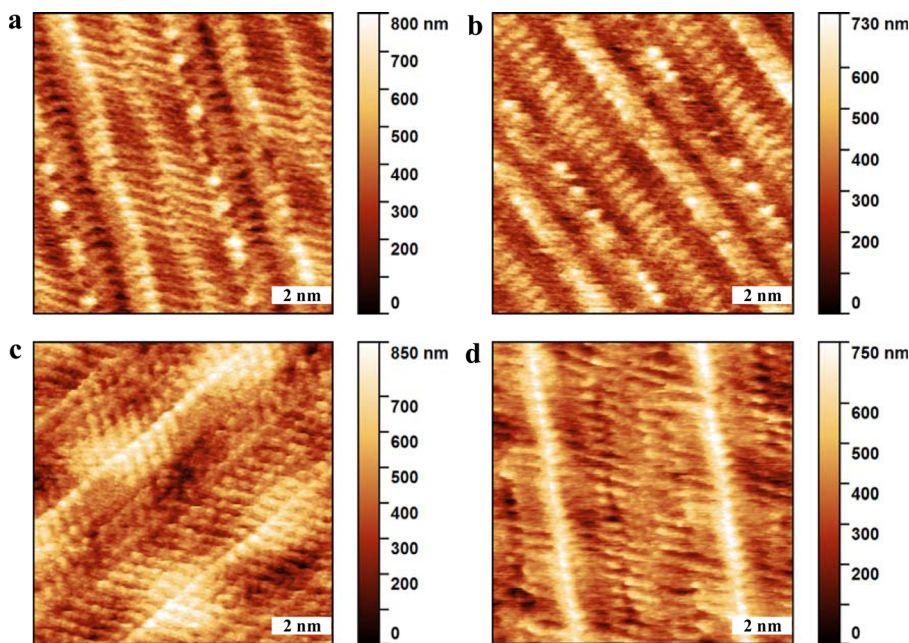**Figure 3.** Scanning tunneling microscopy images of $A\beta_{1-16}$-Cu^{2+} (a,b) and $A\beta_{1-16}$ (c,d). Imaging conditions: (a,b) 10 nm × 10 nm, V_{sample} = 0.55 V, I_{tunnel} = 10 pA; (c) 10 nm × 10 nm, V_{sample} = 0.25 V, I_{tunnel} = 17 pA; (d) 10 nm × 10 nm, V_{sample} = 0.30 V, I_{tunnel} = 14 pA.

Amide III band (1200−1340 cm^{-1}) showed a strong signal at ~1249 cm^{-1}, indicative of $A\beta_{1-16}$ forming either a hydrated β-sheet[61] or a PPII type helical structure[62−64] on the surface. The band at 1449 cm^{-1}, present in the $A\beta_{1-16}$ sample and absent in the $A\beta_{1-16}$-Cu^{2+} sample, belongs to the C−H bending mode vibration of the peptide.[65−68] Increased C−H vibrations in $A\beta_{1-16}$ indicate the lack of intermolecular hydrogen bonding within the peptide; together with increased amide band intensities, it demonstrates that $A\beta_{1-16}$ on the surface is more disordered than $A\beta_{1-16}$-Cu^{2+}.

Scanning Tunneling Microscopy. $A\beta_{1-16}$ is typically a disordered and hydrophilic portion of an extracellular domain of $A\beta$.[23,24,26,68] Because it is a disordered region it has often been omitted from computational studies.[23−27] However, we show here that upon $A\beta_{1-16}$ deposition on HOPG, individual peptide chains laminate into structured β-sheet domains (Figure S2). Previous reports indicate that $A\beta$ has a parallel β-sheet arrangement with amino acids spacings of 0.325 nm.[31,69] For our image analysis, we assumed the same parallel β-sheet arrangement for $A\beta_{1-16}$. The average scanned length of $A\beta_{1-16}$ is 5.2 ± 0.4 nm; this value is consistent with the ideal

$A\beta_{1-16}$ length of 4.875 nm. In addition, we noticed that $A\beta_{1-16}$ has higher structural polymorphism, with the strands' length being less uniform, than that of $A\beta_{1-16}$-Cu^{2+} (Figure S3). These STM studies relied on the deposition from solution of $A\beta_{1-16}$ raising the question of whether there are surface-induced structural changes. Previously, our group has shown that the peptide-surface interactions are relatively small in comparison to the peptide−peptide interactions within the assembly.[21] Furthermore, the transition from the hydrophilic regime to the hydrophobic HOPG surface may mimic the interaction of $A\beta_{1-16}$ with the cellular membrane in physiological conditions.

Based on our measurements, $A\beta_{1-16}$ and $A\beta_{1-16}$-Cu^{2+} vary significantly from one another in terms of their interstrand separations (Figure 2b). Free $A\beta_{1-16}$ peptides have an interstrand separation of 5.8 ± 0.4 Å; this value differs greatly from the interstrand separation in $A\beta_{1-16}$-Cu^{2+}, which is 4.6 ± 0.3 Å. The latter is in a good agreement with $A\beta$ (Figure S4a) and earlier reported literature values for β-sheet separation, which is 4.5−5 Å.[21,69−74] A large interstrand separation value for $A\beta_{1-16}$, together with CD and SERS results, indicates that peptides in that system lack intermolecular hydrogen bonding and are either in a PPII helical configuration or are intrinsically disordered. Intrinsically disordered β-sheets have been identified and previously reported for amyloidogenic peptides.[75−77] However, to our knowledge, there are no structural reports of the interstrand separation for either PPII helices or intrinsically disordered β-sheets. Thus, we cannot conclude which structural state the free $A\beta_{1-16}$ peptides have when deposited on HOPG; all structural characterizations in this study indicate that $A\beta_{1-16}$-Cu^{2+} peptides are in a β-sheet arrangement. This arrangement of $A\beta_{1-16}$-Cu^{2+} is apparently triggered by copper ion binding *between* adjacent $A\beta_{1-16}$ strands. Intercalation of copper ions between strands would cause neighboring β-strands to come into closer contact due to His^+−Cu^{2+} interactions, which are based on the repulsive electrostatic and attractive cation-π interactions between Cu^{2+} and imidazole rings.[78,79]

Topographic examination of the $A\beta_{1-16}$-Cu^{2+} lamellae displayed almost evenly arranged protruding features from both sides of β-sheet boundaries, with one side being more uniform than the other. Such features were present only in $A\beta_{1-16}$-Cu^{2+} and were absent in $A\beta_{1-16}$ (without Cu^{2+}) (Figures 3 and S5; many areas of four independently prepared samples of each were measured; for each distance, the average, standard deviation, and number of measurements used are reported). Both the total lengths of the strands and the distances of the protruding features from both β-sheet boundaries have been measured (Scheme 1). The measured distance of the nonperiodic, site-specific protruding features from the boundary was 0.9 ± 0.1 nm, which corresponds to the protruding features being two to three amino acids away from the β-sheet boundary (Figure 2c,d). The only possible amino acids in the strand, which are two to three amino acids away from the ends of the peptide and can participate in Cu^{2+} binding, are His13 and His14 residues. Adjacent positions of His13 and His14 amino acids in the $A\beta_{1-16}$ strand make them unique in the sequence because only they can participate in binding copper between the strands. Therefore, based on STM image analysis of the protruding features, our results support the conclusion that Cu^{2+} ions bind to His13 and His14 residues forming a histidine brace between two strands. We did not observe nonsite-specific protruding features, suggesting that there are no other Cu^{2+} ions bound on the surface. The measured

Scheme 1. Schematic of the Structure Determined for $A\beta_{1-16}$-Cu^{2+a}
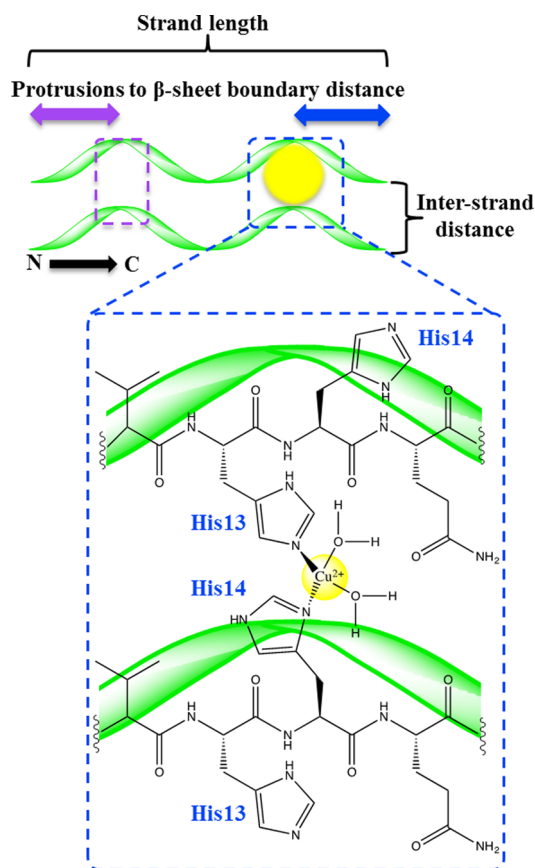
[a] Cu^{2+} interstrand binding to His13 and His14 forms a brace between strands (blue dashed box). In this schematic, we depict copper coordinated with water. It is also possible that copper coordinates with the substrate surface; our data do not distinguish which scenario is more likely. Regular protrusions on STM micrographs that we attribute to be Phe4 are illustrated as a purple dashed box.

distance of the more uniform protruding features from the boundary was 1.0 ± 0.1 nm, which corresponds to the protruding features being three amino acids residues away from the β-sheet boundary. Phenylalanine at the fourth position (Phe4) in the strand is three amino acids away from the beginning of the $A\beta_{1-16}$ strand. We infer that π stacking between the Phe4 ring and graphite leads it to protrude evenly throughout the whole β-sheet domain.

Several previous computational and experimental studies have suggested that neighboring His residues in amyloid peptides or amyloid-like proteins participate in interstrand metal ion binding.[80−86] However, this type of metal ion interaction with $A\beta$ has never previously been observed directly. In this study, based on the length and the position of protruding features of copper ions within $A\beta_{1-16}$ peptides, we show that copper ions participate in interstrand $A\beta_{1-16}$ binding by coordinating with two His residues from adjacent stands.

In conclusion, metal ions are enriched in the β-amyloid aggregates typically found in patients with Alzheimer's dementia, yet their functional role is largely unexplored. Here, we have identified the primary binding site of Cu^{2+} ions to $A\beta_{1-16}$ and have clarified how such Cu^{2+} ions facilitate interstrand binding, implicating metal ions as critical stabilizers

of pathogenic β-amyloid assemblies. Circular dichroism provided key insights into how Cu^{2+} ions interact with the $A\beta_{1-16}$ peptide in solution; inducing a conformational change from a disordered type II helix secondary structure to a secondary structure with β-sheet character. Based on strong C–H bending vibrations and higher PPII helical character in $A\beta_{1-16}$, SERS demonstrated that $A\beta_{1-16}$ peptides on the surface are less densely packed and more disordered than $A\beta_{1-16}$-Cu^{2+}. Finally, scanning tunneling microscopy enabled us to deduce the structural changes of $A\beta_{1-16}$ upon copper binding. In summary, $A\beta_{1-16}$ has a higher structural polymorphism than $A\beta_{1-16}$-Cu^{2+}, as indicated by the range in $A\beta_{1-16}$ strand lengths. When compared to $A\beta_{1-16}$-Cu^{2+}, strands in $A\beta_{1-16}$ are less uniform in the length, suggesting that they sometimes fold in upon themselves. Large interstrand separation in $A\beta_{1-16}$ indicate that such peptides lack hydrogen bonding between adjacent strands. Thus, on a surface, $A\beta_{1-16}$ laminates into either intrinsically disordered β-sheets or into a PPII-type helix. In contrast, our data provide strong evidence that $A\beta_{1-16}$-Cu^{2+} has a smaller interstrand separation and laminates into β-sheets on a surface. We conclude that the interaction of the $A\beta_{1-16}$ peptide with the Cu^{2+} ions is the driving force for this more ordered formation. Lastly, we observed features as apparent protrusions in STM images at the ends of the β-sheet boundaries in $A\beta_{1-16}$-Cu^{2+} but not in $A\beta_{1-16}$. These features are localized 2–3 amino acids away from the β-sheet boundaries, pointing to His13 and His14 as critical binding partners. The only possible amino acids that could participate in copper ion binding that are 2–3 amino acids away from the β-sheet boundary are His13 and His14. These data support the notion that His13 and His14 represent a primary binding site for the copper ions, creating an interstrand histidine brace.

β-Amyloid has been implicated as a primary pathogenic factor in Alzheimer's disease and the current work links metal ions, specifically copper, to the formation and structure of the β-amyloid aggregates that are the signature of this disease. Understanding the structural features of β-amyloid and how it interacts and coassembles with other elements can open the door to studies of β-amyloid aggregates in the tissue environment and the identification of "drugable" targets that ultimately shape the deposition of neurotoxic peptides. Further, blocking metal ion binding could be utilized to destabilize the indigestible β-amyloid clusters in neurodegeneration. (*NB*—As noted above, there may *also* be Cu^{2+} binding sites near the C-terminus of $A\beta_{1-42}$.) This report establishes the capability of scanning tunneling microscopy as a methodology to determine structural characteristics and critical interaction sites in biologically relevant systems where traditional techniques that average or extract only periodic portions of structures have been unsuccessful.[12,21,30,31,72,87,88]

Scanning Probe Microscopy and Surface-Enhanced Raman Spectroscopy Sample Preparation. Solutions were prepared in a glass vial with a final total volume of 400 μL for both samples ($A\beta_{1-16}$ and $A\beta_{1-16}$-Cu^{2+}). $A\beta_{1-16}$ molarity was kept constant between samples: 2.5×10^{-7} M. In the $A\beta_{1-16}$-Cu^{2+} samples, the final Cu^{2+} concentration was 2.5×10^{-5} M. The $A\beta_{1-16}$ solution mixture was prepared by mixing 20 μL of phosphate-buffered saline at pH 7.4, 200 μL of acetonitrile (Sigma-Aldrich Fluka Analytical, St. Louis, MO, purity >99.9%), 179 μL of double-distilled water, and 1 μL of $A\beta_{1-16}$ (American Peptide Company, Inc., Sunnyvale, CA, 95.4% purity). Before depositing $A\beta_{1-16}$ solution onto HOPG (SPI supplies, size: 10 mm × 10 mm × 2 mm) the surface of

HOPG was cleaved with scotch tape to clean the surface and to eliminate any preexisting flakes. $A\beta_{1-16}$ solution was deposited onto HOPG for a 1 min and blown off using nitrogen gas. The $A\beta_{1-16}$-Cu^{2+} solution mixture was prepared by mixing 20 μL of phosphate-buffered saline at pH 7.4, 10 μL of Cu^{2+} (Sigma-Aldrich Fluka Analytical, Copper Standard for ICP 1001 ± 2 mg/L), 200 μL of acetonitrile, 169 μL of double-distilled water, and 1 μL of $A\beta_{1-16}$ solution.

Scanning Tunneling Microscopy Measurements. For STM measurements, a mechanically cut Pt–Ir (80%–20%) (Goodfellow Corp., Oakdale, PA) wire was used as the STM tip. The STM observations were carried out on a Pico SPM microscope head (Molecular Imaging, now Agilent, Santa Clara, CA) controlled by a low-noise controller (RHK Model R9, RHK Technology, Troy, MI) under ambient conditions.

Atomic Force Microscopy Measurements. All AFM measurements were performed under ambient conditions at the California NanoSystems Institute (NanoPico Characterization laboratory) using a Bruker High-Speed MultiMode 8 with ScanAsyst-HR instrument in peak force tapping mode with Bruker Nanoprobe (Model MPP-21100-10, Part RFESP, and nominal force constant 3 N/m).

Scanning Tunneling Microscopy and Atomic Force Microscopy Image Processing. Both STM and AFM images were processed by GWYDDION[88] (free scanning probe microscopy data analysis software). Scratch artifacts were removed from STM images by using MATLAB (Mathworks, Natick, MA) unstripping code (see Supporting Information).

Surface-Enhanced Raman Spectroscopy Measurements. Substrates were prepared as described previously.[48] Briefly, fabrication involved bottom-up templating technology where spin coating and hitting polystyrene (PS) film created PS spheres on Si/SiO$_2$. Polystyrene spheres were used as mask for further gold nanopyramids fabrication. Final gold nanopyramids were approximately 200 nm × 200 nm in size. Graphene was transferred on gold nanopyramids substrates as a final step by chemical vapor deposition. A Renishaw inVia Raman system (Renishaw, IL) operating under ambient conditions was employed for Raman analysis. A 632.8 nm He–Ne laser was used as the Raman excitation source to match the resonant wavelength of the substrate. Laser power and beam diameter were ~5 mW and ~1 μm, respectively. Spectra were acquired by mapping the substrate surface. Each measurement was a convolution of 20 sweeps in the wavelength range of interest with a set integration time of 1 s.

Circular Dichroism Sample Preparation. Solutions were prepared in a glass vial with final total volume of 300 μL for both samples ($A\beta_{1-16}$ and $A\beta_{1-16}$-Cu^{2+}). $A\beta_{1-16}$ molarity kept constant between samples: 7.5×10^{-5} M. In $A\beta_{1-16}$-Cu^{2+} samples, the final Cu^{2+} concentration was 2.5×10^{-5} M. The $A\beta_{1-16}$ solution mixture was prepared by mixing 15 μL of phosphate-buffered saline at pH 7.4, 52.5 μL of acetonitrile, 7.5 μL of double-distilled water, and 225 μL of $A\beta_{1-16}$. The $A\beta_{1-16}$-Cu^{2+} solution mixture was prepared by mixing 15 μL of phosphate-buffered saline at pH 7.4, 7.5 μL of Cu^{2+}, 52.5 μL of acetonitrile, and 225 μL of $A\beta_{1-16}$.

Circular Dichroism Measurements. Circular dichroism (CD) spectra of $A\beta_{1-16}$ and $A\beta_{1-16}$-Cu^{2+} in the wavelength region from 250 to 190 nm were measured at room temperature using a JASCO (Easton, MD) J-715 Circular Dichrosim Spectrophotometer and cell with 1 mm path length. The spectra were recorded with a step resolution of 0.2 nm, scan speed 20 nm/min, bandwidth of 1 nm, sensitivity of 50

mdeg ellipticity, and response 4 s with ten spectra collected and averaged per sample.

Surface-Enhanced Raman Spectroscopy and Circular Dichroism Spectral Analyses. Both SERS and CD spectral analyses, peak assignments, and plotting were carried out using OriginPro software and Microsoft Office Excel.

■ ASSOCIATED CONTENT

Ⓢ Supporting Information

The Supporting Information is available free of charge on the ACS Publications website at DOI: 10.1021/acs.nano-lett.6b02590.

Data and figures that describe circular dichroism results, atomic force microscopy images that show continuous β-sheet monolayers of Aβ_{1-16} and Aβ_{1-16}-Cu^{2+}, scanning tunneling microscopy images with regular patterns of protrusions in the vicinity of the β-sheet boundary, and unstripping MATLAB code that was used to remove horizontal image stripes. (PDF)

■ AUTHOR INFORMATION

Corresponding Authors
*E-mail: psw@cnsi.ucla.edu. Tel.: + 1 (310) 825-0317. (P.S.W.)
*E-mail: jgilles@mail.sdsu.edu. (J.G.)
*E-mail: yhx@ucla.edu. (Y.X.).
*E-mail: yangy@ucla.edu (Y.Y.).

Notes
The authors declare no competing financial interest.

■ ACKNOWLEDGMENTS

■ REFERENCES

(1) Zhu, C. W.; Sano, M. Economic Considerations in the Management of Alzheimer's Disease. *Clin. Interv. Aging* **2006**, *1*, 143−154.

(2) Goldman, L.; Schaffer, A. I. *Goldman's Cecil Medicine*; Elsevier Saunders: Philadelphia, PA, 2011; Chapter 402, pp 2274−2279.

(3) Malakooti, N.; Pritchard, M. A.; Adlard, P. A.; Finkelstein, D. I. Role of Metal Ions in the Cognitive Decline of Down Syndrome. *Front. Aging Neurosci.* **2014**, *6*, 136.

(4) Hyman, B. T.; Van Hoesen, G. W.; Kromer, L. J.; Damasio, A. R. Perforant Pathway Changes and the Memory Impairment of Alzheimer's Disease. *Ann. Neurol.* **1986**, *20*, 472−481.

(5) Lovell, M. A.; Robertson, J. D.; Teesdale, W. J.; Campbell, J. L.; Markesbery, W. R. Copper, Iron, and Zinc in Alzheimer's Disease Senile Plaques. *J. Neurol. Sci.* **1998**, *158*, 47−52.

(6) Budimir, A. Metal Ions, Alzheimer's Disease and Chelation Therapy. *Acta Pharm.* **2011**, *61*, 1−14.

(7) Goure, W. F.; Krafft, G. A.; Jerecic, J.; Hefti, F. Targeting the Proper Amyloid-Beta Neuronal Toxins: A Path Forward for Alzheimer's Disease Immunotherapeutics. *Alzheimer's Res. Ther.* **2014**, *6*, 42.

(8) Chafekar, S. M.; Baas, F.; Scheper, W. Oligomer-Specific Aβ Toxicity in Cell Models is Mediated by Selective Uptake. *Biochim. Biophys. Acta, Mol. Basis Dis.* **2008**, *1782*, 523−531.

(9) Zhao, L. N.; Long, H. W.; Mu, Y.; Chew, L. Y. The Toxicity of Amyloid β Oligomers. *Int. J. Mol. Sci.* **2012**, *13*, 7303−7327.

(10) Danielsson, J.; Pierattelli, R.; Banci, L.; Graslund, A. High-Resolution NMR Studies of the Zinc-Binding Site of the Alzheimer's Amyloid β-Peptide. *FEBS J.* **2007**, *274*, 46−59.

(11) Jun, S.; Gillespie, J. R.; Shin, B.; Saxena, S. The Second Cu(II)-Binding Site in a Proton-rich Environment Interferes with the Aggregation of Amyloid-β(1−40) into Amyloid Fibrils. *Biochemistry* **2009**, *48*, 10724−10732.

(12) Eisenberg, D.; Jucker, M. The Amyloid State of Proteins in Human Diseases. *Cell* **2012**, *148*, 1188−1203.

(13) Minicozzi, V.; Stellato, F.; Comai, M.; Serra, M. D.; Potrich, C.; Meyer-Klaucke, W.; Morante, S. Identifying the Minimal Copper- and Zinc-Binding Site Sequence in Amyloid-β Peptides. *J. Biol. Chem.* **2008**, *283*, 10784−10792.

(14) Xiao, Y.; Ma, B.; McElheny, D.; Parthasarathy, S.; Long, F.; Hoshi, M.; Nussinov, R.; Ishii, Y. Aβ(1−42) Fibril Structure Illuminates Self-Recognition and Replication of Amyloid in Alzheimer's Disease. *Nat. Struct. Mol. Biol.* **2015**, *22*, 499−505.

(15) Streltsov, V. X-ray Absorption and Diffraction Studies of the Metal Binding Sites in Amyloid β-Peptide. *Eur. Biophys. J.* **2008**, *37*, 257−263.

(16) Karr, J. W.; Kaupp, L. J.; Szalai, V. A. Amyloid-Beta Binds Cu^{2+} in a Mononuclear Metal Ion Binding Site. *J. Am. Chem. Soc.* **2004**, *126*, 13534−13538.

(17) Hane, F.; Tran, G.; Attwood, S. J.; Leonenko, Z. Cu^{2+} Affects Amyloid-β (1−42) Aggregation by Increasing Peptide-Peptide Binding Forces. *PLoS One* **2013**, *8*, e59005.

(18) Kepp, K. P. Bioinorganic Chemistry of Alzheimer's Disease. *Chem. Rev.* **2012**, *112*, 5193−5239.

(19) Miller, Y.; Ma, B.; Nussinov, R. Metal Binding Sites in Amyloid Oligomers: Complexes and Mechanisms. *Coord. Chem. Rev.* **2012**, *256*, 2245−2252.

(20) Faller, P.; Hureau, C.; La Penna, G. Metal Ions and Intrinsically Disordered Proteins and Peptides: From Cu/Zn Amyloid-β to General Principles. *Acc. Chem. Res.* **2014**, *47*, 2252−2259.

(21) Claridge, S. A.; Thomas, J. C.; Silverman, M. A.; Schwartz, J. J.; Yang, Y.; Wang, C.; Weiss, P. S. Differentiating Amino Acid Residues and Side Chain Orientations in Peptides Using Scanning Tunneling Microscopy. *J. Am. Chem. Soc.* **2013**, *135*, 18528−18535.

(22) Atwood, C. S.; Moir, R. D.; Huang, X.; Scarpa, R. C.; Bacarra, N. M.; Romano, D. M.; Hartshorn, M. A.; Tanzi, R. E.; Bush, A. I. Dramatic Aggregation of Alzheimer Abeta by Cu(II) is Induced by Conditions Representing Physiological Acidosis. *J. Biol. Chem.* **1998**, *273*, 12817−12826.

(23) Viet, M. H.; Li, M. S. Amyloid Peptide Aβ40 Inhibits Aggregation of Aβ42: Evidence from Molecular Dynamics Simulations. *J. Chem. Phys.* **2012**, *136*, 245105.

(24) Yu, X.; Zheng, J. Polymorphic Structures of Alzheimer's β-Amyloid Globulomers. *PLoS One* **2011**, *6*, e20575.

(25) Miller, Y.; Ma, B.; Nussinov, R. Zinc Ions Promote Alzheimer Aβ Aggregation *via* Population Shift of Polymorphic States. *Proc. Natl. Acad. Sci. U. S. A.* **2010**, *107*, 9490−9495.

(26) Wang, Q.; Wang, Y.; Lu, P. Revealing the Secondary Structural Changes of Amyloid β Peptide by Probing the Spectral Fingerprint Characters. *J. Raman Spectrosc.* **2013**, *44*, 670−674.

(27) Luhrs, T.; Ritter, C.; Adrian, M.; Riek-Loher, D.; Bohrmann, B.; Dobeli, H.; Schubert, D.; Riek, R. 3D Structure of Alzheimer's Amyloid-β(1−42) Fibrils. *Proc. Natl. Acad. Sci. U. S. A.* **2005**, *102*, 17342−17347.

(28) Syme, C. D.; Nadal, R. C.; Rigby, S. E. J.; Viles, J. H. Copper Binding to the Amyloid-β (Aβ) Peptide Associated with Alzheimer's Disease. *J. Biol. Chem.* **2004**, *279*, 18169−18177.

(29) Ma, Q.; Hu, J.; Wu, W.; Liu, H.; Du, J.; Fu, Y.; Wu, Y.; Lei, P.; Zhao, Y.; Li, Y. Characterization of Copper Binding to the Peptide Amyloid-β(1−16) Associated with Alzheimer's Disease. *Biopolymers* **2006**, *83*, 20−31.

(30) Claridge, S. A.; Schwartz, J. J.; Weiss, P. S. Electrons, Photons, and Force: Quantitative Single-Molecule Measurements from Physics to Biology. *ACS Nano* **2011**, *5*, 693−729.

(31) Liu, L.; Niu, L.; Xu, M.; Han, Q.; Duan, H.; Dong, M.; Besenbacher, F.; Wang, C.; Yang, Y. Molecular Tethering Effect of C-Terminus of Amyloid Peptide Aβ42. *ACS Nano* **2014**, *8*, 9503−9510.

(32) Kowalewski, T.; Holtzman, D. M. *In Situ* Atomic Force Microscopy Study of Alzheimer's β-Amyloid Peptide on Different Substrates: New Insights into Mechanism of β-sheet Formation. *Proc. Natl. Acad. Sci. U. S. A.* **1999**, *96*, 3688−3693.

(33) Mattson, M. P.; Cheng, B.; Davis, D.; Bryant, K.; Lieberburg, I.; Rydel, R. E. β-Amyloid Peptides Destabilize Calcium Homeostasis and Render Human Cortical Neurons Vulnerable to Excitotoxicity. *J. Neurosci.* **1992**, *2*, 376−389.

(34) Adzhubei, A. A.; Sternberg, M. J. Left-Handed Polyproline II Helices Commonly Occur in Globular Proteins. *J. Mol. Biol.* **1993**, *229*, 472−493.

(35) Stapley, B. J.; Creamer, T. P. A Survey of Left-Handed Polyproline II Helices. *Protein Sci.* **1999**, *8*, 587−595.

(36) Rucker, A. L.; Creamer, T. P. Polyproline II Helical Structure in Protein Unfolded States: Lysine Peptides Revisited. *Protein Sci.* **2002**, *11*, 980−985.

(37) White, C. J.; Yudin, A. K. Contemporary Strategies for Peptide Macrocyclization. *Nat. Chem.* **2011**, *3*, 509−524.

(38) Han, W. G.; Jalkanen, K. J.; Elstner, M.; Suhai, S. Theoretical Study of Aqueous *N*-Acetyl-L-alanine *N*′-Methylamide: Structures and Raman, VCD and ROA Spectra. *J. Phys. Chem. B* **1998**, *102*, 2587−2602.

(39) Westhof, E. *Water and Biological Macromolecules*; CRC Press: Boca Raton, FL, 1993; Chapter 5, pp 148−162.

(40) Blanch, E. W.; Morozova-Roche, L. A.; Hecht, L.; Noppe, W.; Barron, L. D. Raman Optical Activity Characterization of Native and Molten Globule States of Equine Lysozyme: Comparison with Hen Lysozyme and Bovine α-Lactalbumin. *Biopolymers* **2000**, *57*, 235−248.

(41) Blanch, E. W.; Morozova-Roche, L. A.; Cochran, D. A.; Doig, A. J.; Hecht, L.; Barron, L. D. A Raman Optical Activity Study of the Amyloidogenic Prefibrillar Intermediate of Human Lysozyme. *J. Mol. Biol.* **2000**, *301*, 553−563.

(42) Fandrich, M.; Meinhardt, J.; Grigorieff, N. Structural Polymorphism of Alzheimer Aβ and Other Amyloid Fibrils. *Prion* **2009**, *3*, 89−93.

(43) Chen, Y. R.; Huang, H. B.; Chyan, C. L.; Shiao, M. S.; Lin, T. H.; Chen, Y. C. The Effect of Aβ Conformation on the Metal Affinity and Aggregation Mechanism Studied by Circular Dichroism Spectroscopy. *J. Biochem.* **2006**, *139*, 733−740.

(44) Baldassarre, M.; Barth, A. Pushing the Detection Limit of Infrared Spectroscopy for Structural Analysis of Dilute Protein Samples. *Analyst* **2014**, *139*, 5393−5399.

(45) Goldberg, M. E.; Chaffotte, A. F. Undistorted Structural Analysis of Soluble Proteins by Attenuated Total Reflectance Infrared Spectroscopy. *Protein Sci.* **2005**, *14*, 2781−2792.

(46) Berhanu, W. M.; Hansmann, U. H. Structure and Dynamics of Amyloid-β Segmental Polymorphisms. *PLoS One* **2012**, *7*, e41479.

(47) Baia, M.; Astilean, S.; Iliescu, T. *Raman and SERS Investigations of Pharmaceuticals*; Springer: Berlin, 2008; Chapter 1, pp 9−35.

(48) Wang, P.; Zhang, W.; Liang, O.; Pantoja, M.; Katzer, J.; Schroeder, T.; Xie, Y. Giant Optical Response from Graphene-Plasmonic System. *ACS Nano* **2012**, *6*, 6244−6249.

(49) Radziuk, D.; Möhwald, H. Prospects for Plasmonic Hot Spots in Single Molecule SERS Towards the Chemical Imaging of Live Cells. *Phys. Chem. Chem. Phys.* **2015**, *17*, 21072−21093.

(50) Kumar, C. S. S. R. *Raman Spectroscopy for Nanomaterials Characterization*; Springer: Berlin, 2012; Chapter 10, pp 215−261.

(51) Schweitzer-Stenner, R. Advances in Vibrational Spectroscopy as a Sensitive Probe of Peptide and Protein Structure a Critical Review. *Vib. Spectrosc.* **2006**, *42*, 98−117.

(52) Ayas, S.; Cinar, G.; Ozkan, A. D.; Soran, Z.; Ekiz, O.; Kocaay, D.; Tomak, A.; Toren, P.; Kaya, Y.; Tunc, I.; Zareie, H.; Tekinay, T.; Tekinay, A. B.; Guler, M. O.; Dana, A. Label-Free Nanometer-Resolution Imaging of Biological Architectures Through Surface Enhanced Raman Scattering. *Sci. Rep.* **2013**, *3*, 2624.

(53) Ferrari, A. C. Raman Spectroscopy of Graphene and Graphite: Disorder, Electron-Phonon Coupling, Doping and Nonadiabatic Effects. *Solid State Commun.* **2007**, *143*, 47−57.

(54) Jorio, A.; Martins Ferreira, E. H.; Moutinho, M. V. O.; Stavale, F.; Achete, C. A.; Capaz, R. B. Measuring Disorder in Graphene with G and D Bands. *Phys. Status Solidi B* **2010**, *247*, 2980−2982.

(55) Siddhanta, S.; Naray, C. Surface Enhanced Raman Spectroscopy of Proteins: Implications for Drug Designing. *Nanomater. Nanotechnol.* **2012**, *2*, 1.

(56) Barth, A. Infrared Spectroscopy of Proteins. *Biochim. Biophys. Acta, Bioenerg.* **2007**, *1767*, 1073−1101.

(57) Siddhanta, S.; Karthigeyan, D.; Kundu, P. P.; Kundu, T. K.; Narayana, C. Surface Enhanced Raman Spectroscopy of Aurora Kinases: Direct, Ultrasensitive Detection of Autophosphorylation. *RSC Adv.* **2013**, *3*, 4221−4230.

(58) Podstawka, E.; Ozaki, Y.; Proniewicz, L. M. Part II: Surface-Enhanced Raman Spectroscopy Investigation of Methionine Containing Heterodipeptides Absorbed on Colloidal Silver. *Appl. Spectrosc.* **2004**, *58*, 581−590.

(59) Schmidt, E. A. Spectroscopic Investigation of the Beta-Amyloid Peptide. Ph.D. Dissertation, University of Missouri, Columbia, MO, 2008.

(60) Di Foggia, M.; Taddei, P.; Torreggiani, A.; Dettin, M.; Tinti, A. Interaction between Oligopeptides and Oxidised Titanium Surfaces Detected by Vibrational Spectroscopy. *J. Raman Spectrosc.* **2011**, *42*, 276−285.

(61) Shashilov, V.; Xu, M.; Makarava, N.; Savtchenko, R.; Baskakov, I. V.; Lednev, I. K. Dissecting Structure of Prion Amyloid Fibrils by Hydrogen-Deuterium Exchange Ultraviolet Raman Spectroscopy. *J. Phys. Chem. B* **2012**, *116*, 7926−7930.

(62) Oladepo, S. A.; Xiong, K.; Hong, Z.; Asher, S. A.; Handen, J.; Lednev, I. K. UV Resonance Raman Investigations of Peptide and Protein Structure and Dynamics. *Chem. Rev.* **2012**, *112*, 2604−2628.

(63) Ahmed, Z.; Beta, I. A.; Mikhonin, A. V.; Asher, S. A. UV-Resonance Raman Thermal Unfolding Study of Trp-Cage Shows That It Is Not A Simple Two State Miniprotein. *J. Am. Chem. Soc.* **2005**, *127*, 10943−10950.

(64) Mikhonin, A. V.; Myshakina, N. S.; Bykov, S. V.; Asher, S. A. UV-Resonance Raman Determination of Polyproline II, Extended 2.5₁-Helix, and β-Sheet Ψ Angle Energy Landscape in Poly-L-Lysine and Poly-L-Glutamic Acid. *J. Am. Chem. Soc.* **2005**, *127*, 7712−7720.

(65) Ma, C. Y.; Rout, M. K.; Chan, W. M.; Phillips, D. L. Raman Spectroscopic Study of Oat Globulin Conformation. *J. Agric. Food Chem.* **2000**, *48*, 1542−1547.

(66) Camerlingo, C.; d'Apuzzo, F.; Grassia, V.; Perillo, L.; Lepore, M. Micro-Raman Spectroscopy for Monitoring Changes in Periodontal Ligaments and Gingival Crevicular Fluid. *Sensors* **2014**, *14*, 22552−22563.

(67) Kurouski, D.; Van Duyne, R. P.; Lednev, I. K. Exploring the Structure and Formation Mechanism of Amyloid Fibrils by Raman Spectroscopy: A Review. *Analyst* **2015**, *140*, 4967−4980.

(68) Phillips, J. C. Thermodynamic Description of Beta Amyloid Formation Using Physicochemical Scales and Fractal Bioinformatic Scales. *ACS Chem. Neurosci.* **2015**, *6*, 745−750.

(69) Mao, X.; Guo, Y.; Luo, Y.; Niu, L.; Liu, L.; Ma, X.; Wang, H.; Yang, Y.; Wei, G.; Wang, C. Sequence Effects on Peptide Assembly Characteristics Observed by Using Scanning Tunneling Microscopy. *J. Am. Chem. Soc.* **2013**, *135*, 2181−2187.

(70) Nelson, R.; Sawaya, M. R.; Balbirnie, M.; Madsen, A. O.; Riekel, C.; Grothe, R.; Eisenberg, D. Structure of the Cross-β Spine of Amyloid-Like Fibrils. *Nature* **2005**, *435*, 773−778.

(71) Shaytan, A. K.; Schillinger, E. K.; Mena-Osteritz, E.; Schmid, S.; Khalatur, P. G.; Bauerle, P.; Khokhlov, A. R. Self-Organizing Bioinspired Oligothiophene-Oligopeptide Hybrids. *Beilstein J. Nanotechnol.* **2011**, *2*, 525−544.

(72) Mao, X. B.; Wang, C. X.; Wu, X. K.; Ma, X. J.; Liu, L.; Zhang, L.; Niu, L.; Guo, Y. Y.; Li, D. H.; Yang, Y. L.; Wang, C. Beta Structure Motifs of Islet Amyloid Polypeptides Identified Through Surface-Mediated Assemblies. *Proc. Natl. Acad. Sci. U. S. A.* **2011**, *108*, 19605−19610.

(73) Paravastu, A. K.; Leapman, R. D.; Yau, W. M.; Tycko, R. Molecular Structural Basis for Polymorphism in Alzheimer's β-Amyloid Fibrils. *Proc. Natl. Acad. Sci. U. S. A.* **2008**, *105*, 18349−18354.

(74) Makin, O. S.; Atkins, E.; Sikorski, P.; Johansson, J.; Serpell, L. C. Molecular Basis for Amyloid Fibril Formation and Stability. *Proc. Natl. Acad. Sci. U. S. A.* **2005**, *102*, 315−320.

(75) Dong, J.; Lu, K.; Lakdawala, A.; Mehta, A. K.; Lynn, D. G. Controlling Amyloid Growth in Multiple Dimensions. *Amyloid* **2006**, *13*, 206−215.

(76) Morgan, D. M.; Lynn, D. G.; Lakdawala, A. S.; Snyder, J. P.; Liotta, D. C. Amyloid Structure: Models and Theoretical Considerations in Fibrous Aggregates. *J. Chin. Chem. Soc.* **2002**, *49*, 459−466.

(77) Lakdawala, A. S.; Morgan, D. M.; Liotta, D. C.; Lynn, D. G.; Snyder, J. P. Dynamics and Fluidity of Amyloid Fibrils: A Model of Fibrous Protein Aggregates. *J. Am. Chem. Soc.* **2002**, *124*, 15150−15151.

(78) Liao, S. M.; Du, Q. S.; Meng, J. Z.; Pang, Z. W.; Huang, R. B. The Multiple Roles of Histidine in Protein Interactions. *Chem. Cent. J.* **2013**, *7*, 44.

(79) Jones, C. E.; Abdelraheim, S. R.; Brown, D. R.; Viles, J. H. Preferential Cu^{2+} Coordination by His^{96} and His^{111} Induces β-Sheet Formation in the Unstructured Amyloidogenic Region of the Prion Protein. *J. Biol. Chem.* **2004**, *279*, 32018−32027.

(80) Gamez, P.; Caballero, A. B. Copper in Alzheimer's Disease: Implications in Amyloid Aggregation and Neurotoxicity. *AIP Adv.* **2015**, *5*, 092503.

(81) Morgan, D. M.; Dong, J.; Jacob, J.; Lu, K.; Apkarian, R. P.; Thiyagarajan, P.; Lynn, D. G. Metal Switch for Amyloid Formation: Insight into the Structure of the Nucleus. *J. Am. Chem. Soc.* **2002**, *124*, 12644−12645.

(82) Faller, P. Copper and Zinc Binding to Amyloid-Beta: Coordination, Dynamics, Aggregation, Reactivity and Metal-Ion Transfer. *ChemBioChem* **2009**, *10*, 2837−2845.

(83) Rufo, C. M.; Moroz, Y. S.; Moroz, O. V.; Stohr, J.; Smith, T. A.; Hu, X.; DeGrado, W. F.; Korendovych, I. V. Short Peptides Self-Assemble to Produce Catalytic Amyloids. *Nat. Chem.* **2014**, *6*, 303−309.

(84) Istrate, A. N.; Kozin, S. A.; Zhokhov, S. S.; Mantsyzov, A. B.; Kechko, O. I.; Pastore, A.; Makarov, A. A.; Polshakov, V. I. Interplay of Histidine Residues of the Alzheimer's Disease Aβ Peptide Governs Its Zn-induced Oligomerization. *Sci. Rep.* **2016**, *6*, 21734.

(85) Hernández-Guzmán, J.; Sun, Li.; Mehta, A. K.; Dong, J.; Lynn, D. G.; Warncke, K. Copper(II)-bis-Histidine Coordination Structure in Fibrillar Amyloid-β Peptide Fragment and Model Complexes Revealed by using Electron Spin Echo Envelope Modulation Spectroscopy. *ChemBioChem* **2013**, *14*, 1762−1771.

(86) Dong, J.; Canfield, J.; Mehta, A. K.; Shokes, J. E.; Tian, B.; Childers, S.; Simmons, J. A.; Mao, Z.; Scott, R. A.; Warncke, K.; Lynn, D. G. Engineering Metal Ion Coordination to Regulate Amyloid Fibril Assembly and Toxicity. *Proc. Natl. Acad. Sci. U. S. A.* **2007**, *104*, 13313−13318.

(87) Yu, Y.; Yang, Y.; Wang, C. Site-Specific Analysis of Amyloid Assemblies by Using Scanning Tunneling Microscopy. *Chin. J. Chem.* **2015**, *33*, 24−34.

(88) Nečas, D.; Klapetek, P. Gwyddion: An Open-Source Software for SPM Data Analysis. *Cent. Eur. J. Phys.* **2012**, *10*, 181−188.